On the Chemical Bonding of Gold in Auro-Boron Oxide Clusters Au_nBO^- ($n = 1-3$)

Dmitry Yu. Zubarev and Alexander I. Boldyrev*

Department of Chemistry and Biochemistry, Utah State University, Logan, Utah 84322-0300

Jun Li*

W. R. Wiley Environmental Molecular Sciences Laboratory, Pacific Northwest National Laboratory, MS K8-91, P. O. Box 999, Richland, Washington 99352

Hua-Jin Zhai and Lai-Sheng Wang*

Department of Physics, Washington State University, 2710 University Drive, Richland, Washington 99354, and Chemical Sciences Division, Pacific Northwest National Laboratory, MS K8-88, P. O. Box 999, Richland, Washington 99352

During experiment on Au–B alloy clusters, an auro–boron oxide cluster Au_2BO^- was observed to be an intense peak dominating the Au–B mass spectra, along with weaker signals for $AuBO^-$ and Au_3BO^-. Well-resolved photoelectron spectra have been obtained for the three new oxide clusters, which exhibit an odd–even effect in electron affinities. Au_2BO^- is shown to be a closed shell molecule with a very high electron detachment energy, whereas $AuBO$ and Au_3BO neutrals are shown to be closed shell species with large HOMO-LUMO gaps, resulting in relatively low electron affinities. Density functional calculations were performed for both Au_nBO^- ($n = 1-3$) and the corresponding H_nBO^- species to evaluate the analogy between bonding of gold and hydrogen in these clusters. The combination of experiment and theory allowed us to establish the structures and chemical bonding of these tertiary clusters. We find that the first gold atom does mimic hydrogen and interacts with the BO unit to produce a linear $AuBO$ structure. This unit preserves its identity when interacting with additional gold atoms: a linear $Au^-[AuBO]$ complex is formed when adding one extra Au atom and two isomeric $Au_2^-[AuBO]$ complexes are formed when adding two extra Au atoms. Since BO^- is isoelectronic to CO, the Au_nBO^- species can be alternatively viewed as Au_n interacting with a BO^- unit. The structures and chemical bonding in Au_nBO^- are compared to those in the corresponding Au_nCO complexes.

1. Introduction

A gold phosphine unit ($AuPPh_3$) is known to participate in chemical interactions analogous to that of hydrogen. For instance, substitution of covalently bound hydrogen with $AuPPh_3$ results in the same geometry structures in some compounds. This phenomenon made it possible to interpret various gold–carborane complexes.[1,2] Gold-containing *closo*-carboranes reported by Mitchel and Stone,[1a] Reid and Welch,[1b] and Baukova et al.[1c] represent substances where gold forms classical two-center two-electron (2c-2e) bonds with carbon. Cluster bonding between $AuPPh_3$ and *nido*-carboranes was encountered in substances synthesized and characterized by Stone and co-workers.[1d–h] Experimental work of Hawthorne and co-workers[1i] demonstrated that in aurocarboranes atoms of gold can interact with each other as well as form 2c-2e bonds with carbon. Gold-tin-*closo*-borate compounds synthesized and characterized by Wesemann and co-workers have Sn–Au bonds.[2] More detailed information on Au–B compounds can be found in a recent review.[3]

The analogy between hydrogen and $AuPPh_3$ indeed goes beyond carboranes and gives rise to various compounds with 2c-2e C–Au, N–Au, and B–Au bonds.[4,5] C–AuPPh_3 bonds

are encountered in compounds containing the hypercoordinated pentagonal-bypiramidal $C(AuPPh_3)_5^+$ and octahedral $C(AuPPh_3)_6^{2+}$ cations.[5b] Model systems $BH_n(AuPH_3)_m^k$, where $n + m = 3$ or 4, and charge k is $-2, ..., +1$,[5c] and model complexes $[(LAu)_6X_m]^{m+}$, $[(LAu)_5X_m]^{(m-1)+}$, and $[(LAu)_4X_m]^{(m-2)+}$ (with central atoms $X_1 = B$, $X_2 = C$, and $X_3 = N$ and ligands $L = PH_3$ or $P(CH_3)_3$)[5d] have been studied theoretically to evaluate the stabilizing effect of $Au–PR_3$ interactions in these systems. Pyykkö et al.[5e] investigated the effect of $Au–PR_3$ interaction on chemical bonding in $X(AuPPh_3)_n^{m+}$ systems by considering pure XAu_n^{m+} clusters. The boron-centered gold cluster in the $[(Cy_3P)B((AuPPh_3)_4]^+BF_4^-$ salt have been synthesized and characterized by Schmidbaur and co-workers.[5f] Gold diboride AuB_2 compounds, which have hexagonal layers of boron atoms with gold atoms in between, are well-known as well.[5g–j]

The analogy of chemical bonding between a bare gold atom and H has been recently discovered in some binary Au clusters produced in molecular beams.[6–8] First, $SiAu_4$ and $SiAu_n$ ($n = 2, 3$) were demonstrated to have structures and bonding similar to the silane SiH_4 and SiH_n, respectively.[6] Subsequent studies of Si_2Au_n ($n = 2$ and 4) and Si_3Au_3 clusters revealed their similarity to Si_2H_n ($n = 2$ and 4) and Si_3H_3, respectively.[7] B–Au bonds in the $Au_2B_7^-$ cluster[8] turned out to be covalent and similar to the B–H bonds in the $B_7H_2^-$ cluster.[9] Very recently, we have used the concept of Au/H analogy to consider the

* Corresponding author. E-mail: boldyrev@cc.usu.edu (A.I.B.); jun.li@pnl.gov (J.L.); ls.wang@pnl.gov (L.S.W.).

Chemical Bonding of Au in Au$_n$BO⁻ Clusters

J. Phys. Chem. A, Vol. 111, No. 9, 2007 **1649**

possibility of deltahedral *closo*-auro-boranes B$_n$Au$_n^{2-}$ analogous to spherically aromatic *closo*-boranes B$_n$H$_n^{2-}$ ($n = 5-12$).[10] The challenging question is how far the Au/H analogy can go in determining the structure and chemical bonding in other mixed clusters containing Au. Oxides of boron hydrides have been studied computationally previously[11] and can be used as reference systems in further exploration of the Au/H analogy.

On the other hand, highly dispersed gold nanoparticles are known to exhibit high catalytic activity in the reaction of low-temperature CO oxidation,[12] which made the research of gold clusters extremely attractive.[13] Elucidation of the nature and mechanisms of the catalytic activity of nanogold has become a subject of significant scientific efforts.[14−24] While the role of the oxide support is important in nanogold catalysis,[13] there is evidence that the high catalytic activity of nanogold is not based on the presence of a substrate.[15] Therefore, chemisorbed gold cluster complexes can be viewed as molecular models of nanogold catalysts. The fact that BO⁻ anion and CO molecule are valent isoelectronic suggests that auro-boron oxides can be used as a model system to provide further insight into the mechanisms of CO chemisorption on nanogold and nanogold catalytic properties. Studies of the interaction of CO molecules with gold clusters and gold nanoparticles have been carried out,[25−29] revealing pronounced size dependence and chemisorption saturation. Such complexes as Au(CO)$_n$ ($n = 1-5$) and Au$_n$(CO)$_2$ ($n = 1, 2$) have been assigned in the study of infrared spectra of Au−CO complexes formed in a rare gas matrix.[29] Zhai and Wang observed several series of gold carbonyl cluster anions Au$_m$(CO)$_n^-$ ($m = 2-5$, $n = 1-7$) in the gas phase and characterized their electronic structure using photoelectron spectroscopy (PES).[30] It was reported that for a given gold cluster CO adsorption reaches a critical number of saturation that corresponds exactly to the number of available low coordination apex sites of the respective bare gold clusters. In a subsequent work,[31] Wang and co-workers reported a combined PES and ab initio investigation of CO chemisorption on the planar triangular gold hexamer, Au$_6$(CO)$_n^-$ ($n = 1-3$). They showed that the three CO molecules bind to the three apex sites with little structural distortion to the triangular Au$_6$ parent.

In the current paper a series of auro-borane oxides Au$_n$BO⁻ ($n = 1-3$) has been studied by using a combination of PES and density functional calculations. Structures of the corresponding atomic assemblies are established based on the agreement between experimental and theoretical photoelectron spectra. It turns out that the boron atom of the BO fragment tends to bind with one rather than two gold atoms. Because of this, the BO⁻ unit behaves as a monodentate ligand with respect to gold, similar to CO interactions with Au clusters. Analyses of molecular orbitals (MO) and natural bond orbitals (NBO) were carried out to reveal the nature of the chemical bonding in the auro-boron oxides.

2. Experimental and Computational Methods

2.1. Photoelectron Spectroscopy. The experiment was carried out using a magnetic-bottle-type PES apparatus equipped with a laser vaporization supersonic cluster source. Details of the apparatus have been described elsewhere.[32,33] Briefly, the Au$_n$BO⁻ ($n = 1-3$) mixed cluster anions were produced by laser vaporization of a ¹⁰B/Au mixed target in the presence of a pure helium carrier gas during experiments aimed at Au−B binary alloy clusters.[8] In addition to the desired Au/B alloy clusters, the Au$_2$BO⁻ species appeared to be a particularly intense impurity peak in typical time-of-flight mass spectra and drew our attention. The oxygen impurity was most likely from

the target, which was pressed from a mixture of Au and isotopically enriched ¹⁰B powders. We further noted that two other oxide impurities, Au$_n$BO⁻ ($n = 1, 3$), were also present, albeit at lower abundance than Au$_2$BO⁻. These impurity clusters were carefully studied to elucidate their structure and bonding. They were each mass-selected and decelerated before being photodetached by a pulsed laser beam. Photoelectrons were collected at nearly 100% efficiency by a magnetic bottle and analyzed in a 3.5 m long electron flight tube. The photodetachment experiment was conducted at four detachment photon energies: 532 (2.331 eV), 355 (3.496 eV), 266 (4.661 eV), and 193 nm (6.424 eV). The PES spectra were calibrated by using the known spectra of Au⁻ and Rh⁻, and the energy resolution of the apparatus was $\Delta E_k/E_k \approx 2.5\%$, that is, approximately 25 meV for 1 eV electrons.

2.2. Computational Methods. We used the hybrid B3LYP method[34] with LANL2DZ[35] pseudopotential and basis sets for the preliminary determination of the stationary points on the potential energy surface. The obtained results were refined by using Stuttgart relativistic small-core pseudopotential and valence basis set[36] augmented with two f and one g function on gold (SDD hereafter) and aug-cc-pVTZ (AVTZ hereafter)[37] basis set on boron and oxygen. Computations of the structures of H$_n$BO⁻ ($n = 1-3$) were performed at the B3LYP/AVTZ level of theory for comparison with the Au$_n$BO⁻ systems.

Theoretical vertical detachment energies (VDEs) were calculated by using time-dependent (TD) density functional theory[38] at the B3LYP/SDD+AVTZ (at the optimized B3LYP/SDD+AVTZ geometries) level, which proved to be an inexpensive and reliable method for gold clusters and complexes.[39] In this approach, the VDEs were calculated via the lowest transitions from the ground electronic state of the anion into the ground state of the neutral species (at the B3LYP level of theory) and the vertical excitation energies in the neutral species (at the TD-B3LYP level of theory) at the anion geometry.

Chemical bonding was investigated by means of natural bond orbital (NBO 5.0)[40] and molecular orbital analyses. The Gaussian 03[41] and NWChem[42] software packages were used throughout this project. The MOLDEN 3.4[43] program was chosen for the visualization of the molecular orbitals.

3. Experimental Results

The PES spectra at various photon energies are shown in Figures 1−3 for Au$_n$BO⁻ ($n = 1-3$), respectively. The observed adiabatic and vertical detachment energies (ADEs and VDEs) are summarized in Table 1 and compared to theoretical results to be described.

3.1. AuBO⁻. The 532 nm spectrum of AuBO⁻ (Figure 1a) revealed a partially resolved vibrational progression for the ground state transition (X) with a spacing of 430 ± 40 cm⁻¹. The 0−0 transition defines the electron affinity (EA) of 1.46 ± 0.02 eV for the AuBO neutral molecule, whereas the 1 ← 0 transition at 1.51 ± 0.02 eV represents the ground state VDE of the anion. No additional transitions were accessible at higher binding energies in the 355 (Figure 1b) and 266 nm spectra (not shown). The first excited state (A) of AuBO turned out to be located at a rather high binding energy of 4.78 ± 0.03 eV and was only accessed at 193 nm along with more features beyond 5 eV (Figure 1c). The ADE difference between features X and A defines a large excitation energy (3.27 eV) for the first excited state of AuBO, which can also be viewed as the HOMO-LUMO gap for the AuBO molecule. This HOMO-LUMO gap for AuBO is substantially greater than that for any bare gold clusters[39,44] or bare boron clusters,[45] suggesting that

1650 *J. Phys. Chem. A, Vol. 111, No. 9, 2007*

Zubarev et al.
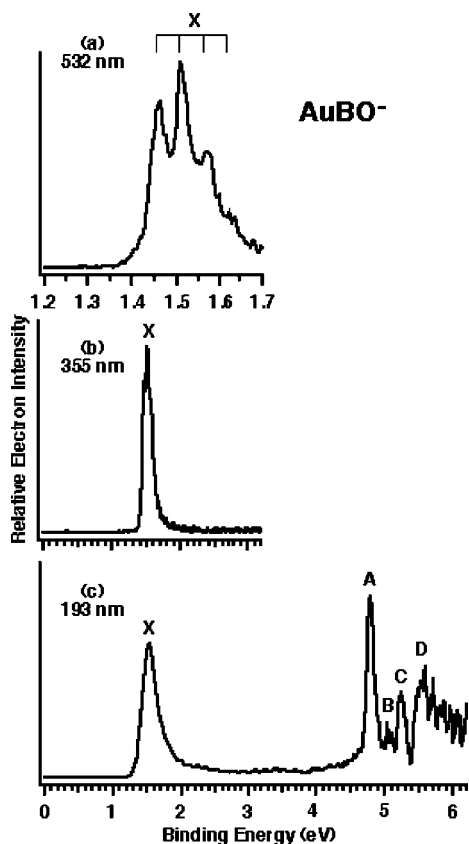
Figure 1. Photoelectron spectra of AuBO⁻ at (a) 532, (b) 355, and (c) 193 nm. Vertical bars in part a represent vibrational structures.
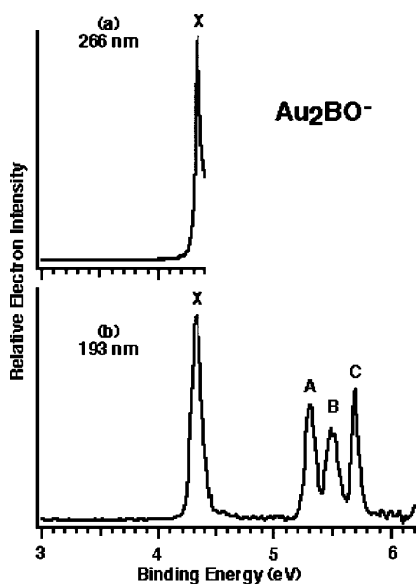
Figure 2. Photoelectron spectra of Au_2BO^- at (a) 266 and (b) 193 nm.

Figure 3. Photoelectron spectra of Au_3BO^- at (a) 355, (b) 266, and (c) 193 nm.

AuBO is a very stable closed shell molecule. The features beyond 5.0 eV were more congested and three well-defined bands were discernible: B (5.07 ± 0.05 eV), C (5.26 ± 0.03 eV), and D (5.55 ± 0.05 eV).

3.2. Au₂BO⁻. The electron affinity of Au_2BO^- was found to be extremely high and only 266 and 193 nm photons were able to induce electron detachment; as shown in Figure 2a, a sharp ground state transition (X) was observed in the 266 nm spectrum with a VDE of 4.33 ± 0.02 eV. Since no vibrational structures were resolved, the ground state ADE was estimated by drawing a straight line along the leading edge of the X band and then adding the instrumental resolution to the intersection with the binding energy axis. The ADE thus evaluated is 4.32 ± 0.02 eV, which also represents the electron affinity of the Au_2BO neutral species. The extremely high electron affinity suggests that the Au_2BO neutral is an open shell system, resulting in a highly stable closed-shell Au_2BO^- anion and its special mass abundance in our cluster source. The 193 nm spectrum (Figure 2b) further revealed three well-resolved features: A (VDE: 5.31 ± 0.02 eV), B (VDE: 5.50 ± 0.03 eV), and C (VDE: 5.69 ± 0.02 eV). The band B appeared to be broader and contain a shoulder on the higher binding energy side, whereas bands X, A, and C were relatively sharp. The overall PES pattern of Au_2BO^- is quite simple, consistent with the closed-shell nature of this anion.

3.3. Au₃BO⁻. Au_3BO^- also exhibits a rather high electron affinity (Figure 3), although it is much lower than that of Au_2BO^-. The 355 nm spectrum revealed only the ground state transition X with a VDE of 3.13 ± 0.02 eV and ADE of 3.08 ± 0.02 eV, which also defines the EA of neutral Au_3BO. A broad shoulder (labeled X′) was observed at ∼3.4 eV in the 266 nm spectrum, but it became very weak at 193 nm, suggesting it was likely due to a minor isomer, as borne out from our theoretical calculations (vide infra). Numerous additional spectral features were observed at higher binding energies in the 193 nm spectrum (Figure 3c) and were reasonably well-resolved. In particular, the first excited state A is located at a rather high binding energy of 4.96 ± 0.03 eV, defining a large HOMO-LUMO gap of 1.83 eV for the Au_3BO neutral cluster. Beyond band A, the spectrum appears to be congested. Nevertheless, numerous well-defined sharp bands were resolved: B (5.11 ± 0.05 eV), C (5.29 ± 0.03 eV), D (5.56 ± 0.03 eV), E (5.68 ± 0.03 eV), and F (5.80 ± 0.02 eV).

Chemical Bonding of Au in Au$_n$BO$^-$ Clusters

J. Phys. Chem. A, Vol. 111, No. 9, 2007 **1651**

TABLE 1: Experimental and Theoretical Vertical Detachment Energies (in eV) for Au$_n$BO$^-$ ($n = 1-3$)

species	feature	ADE (exptl)	VDE (exptl)	final configuration	TD-B3LYP/ SDD+AVTZ
AuBO$^-$ $C_{\infty v}$ ($^2\Sigma^+$)	X	1.46 ± 0.02	1.51 ± 0.02	$^1\Sigma^+$ ($1\delta^4 4\sigma^2 5\sigma^0$)	1.48
	A		4.78 ± 0.03	$^3\Sigma^+$ ($1\delta^4 4\sigma^1 5\sigma^1$)	4.56
	B		5.07 ± 0.05		
	C		5.26 ± 0.03	$^1\Sigma^+$ ($1\delta^4 4\sigma^1 5\sigma^1$)	5.33
	D		5.55 ± 0.05		
Au$_2$BO$^-$ $C_{\infty v}$ ($^1\Sigma^+$)	X	4.32 ± 0.02	4.33 ± 0.02	$^2\Sigma^+$ ($2\delta^4 3\pi^4 5\sigma^2 6\sigma^1$)	4.08
	A		5.31 ± 0.02	$^2\Sigma^+$ ($2\delta^4 3\pi^4 5\sigma^1 6\sigma^2$)	5.19
	B		5.50 ± 0.03	$^2\Pi$ ($2\delta^4 3\pi^3 5\sigma^2 6\sigma^2$)	5.56
	C		5.69 ± 0.02	$^2\Delta$ ($2\delta^3 3\pi^4 5\sigma^2 6\sigma^2$)	5.86
Au$_3$BO$^-$ C_{2v} (^{2}B$_2$)	X	3.08 ± 0.02	3.13 ± 0.02	^{1}A$_1$ ($3a_2^2 5b_2^2 9a_1^2 6b_2^0$)	3.07
	A		4.96 ± 0.03	^{3}B$_2$ ($4b_2^2 3a_2^2 5b_2^2 9a_1^1 6b_2^1$)	4.77
	B		5.11 ± 0.05	^{1}B$_2$ ($4b_2^2 3a_2^2 5b_2^2 9a_1^1 6b_2^1$)	4.90
	C		5.29 ± 0.03	^{3}A$_1$ ($4b_2^2 3a_2^2 5b_2^1 9a_1^2 6b_2^1$)	5.34
	D		5.56 ± 0.03	^{3}B$_1$ ($4b_2^2 3a_2^1 5b_2^2 9a_1^2 6b_2^1$)	5.64
	E		5.68 ± 0.03	^{3}A$_1$ ($4b_2^1 3a_2^2 5b_2^2 9a_1^2 6b_2^1$)	5.73
	F		5.80 ± 0.02	^{1}A$_1$ ($4b_2^2 3a_2^2 5b_2^1 9a_1^2 6b_2^1$)	5.75
Au$_3$BO$^-$ C_s (^{2}A$'$)	X$'$		~ 3.4	^{1}A$'$ ($13a'^2 14a'^2 15a'^0$)	3.67
				^{3}A$'$ ($13a'^2 14a'^1 15a'^1$)	4.89
				^{1}A$'$ ($13a'^2 14a'^1 15a'^1$)	5.51
				^{3}A$'$ ($13a'^1 14a'^2 15a'^1$)	5.60
				^{1}A$'$ ($13a'^1 14a'^2 15a'^1$)	5.85

4. Theoretical Results

4.1. AuBO$^-$ and HBO$^-$. The most stable $C_{\infty v}$ ($^2\Sigma^+$) structure I of AuBO$^-$ is presented in Figure 4a and Table 2. The geometry of the lowest energy $C_{\infty v}$ ($^2\Sigma^+$) structure II of HBO$^-$ (Figure 4a) is consistent with previous results obtained for the neutral species,[11] but the anion is unstable toward the spontaneous electron detachment (ADE = −0.58 eV at the level of B3LYP/AVTZ). Search for $C_{\infty v}$ structures of AuOB$^-$ and HOB$^-$ where the gold/hydrogen atom is bound to the oxygen atom in both cases resulted in second-order saddle points. Further optimization along the doubly degenerate imaginary vibrational mode led to the $C_{\infty v}$ ($^2\Sigma^+$) structure I in the case of AuBO$^-$. In the case of HBO$^-$ we obtained a bent C_s (^{2}A$'$) isomer III that is 38.6 kcal/mol higher than the $C_{\infty v}$ ($^2\Sigma^+$) structure II.

4.2. Au$_2$BO$^-$ and H$_2$BO$^-$. The ground state of Au$_2$BO$^-$ has a linear $C_{\infty v}$ ($^1\Sigma^+$) structure IV (Figure 4b and Table 2). The energetically closest C_{2v} ^{1}A$_1$ isomer (structure V, Figure 4b) is 25.0 kcal/mol less stable. On the contrary, the C_{2v} ^{1}A$_1$ structure VI of H$_2$BO$^-$ is the most stable isomer. H$_2$BO$^-$ also has two higher energy isomers with $C_{\infty v}$ symmetry. The first one is the $C_{\infty v}$ ($^1\Sigma^+$) structure VII (E_{relative} = 20.4 kcal/mol) that represents a van der Waals complex between H$_2$ and BO$^-$. The second one is the $C_{\infty v}$ ($^1\Sigma^+$) structure VIII (E_{relative} = 41.6 kcal/mol) that corresponds to a van der Waals complex of H$^-$ and HBO. The different energetic preference of the isomers, or the tendency of the boron atom of the BO fragment to bind to one atom of gold (monodentate behavior) but to two atoms of hydrogen (bidentate behavior), is remarkable and will be considered in detail in the chemical bonding section (see below).

H$_2$BO$^-$ also has stable cis and trans configurations where one hydrogen atom is bound to the boron atom and the other to the oxygen atom (structures IX and X, Figure 4b). The trans-isomer IX (C_s ^{1}A$'$) is found to be 56.2 kcal/mol higher than the ground state structure VI and the cis-isomer X (C_s ^{1}A$'$) is 60.0 kcal/mol higher. Analogous isomers of Au$_2$BO$^-$ were not found in our search. When starting from the corresponding cis and trans configurations of Au$_2$BO$^-$, our optimization led to the ground state structure IV or to an unbound Au atom and AuBO$^-$.

4.3. Au$_3$BO$^-$ and H$_3$BO$^-$. The C_{2v} (^{2}B$_2$) structure XI (Figure 4c, Table 2) was found to be the most stable isomer for Au$_3$BO$^-$. The next isomer, the C_s (^{2}A$'$) structure XII (Figure 4c, Table 2), is only 1.0 kcal/mol higher in energy and is expected to

contribute to the photoelectron spectrum of Au$_3$BO$^-$. Again, while in the ground state of Au$_3$BO$^-$ the boron atom behaves in a monodentate manner toward gold: it exhibits bidentate behavior toward hydrogen in the C_s (^{2}A$'$) global minimum structure XVI of H$_3$BO$^-$ (Figure 4c). The anionic C_s (^{2}A$'$) H$_3$BO$^-$ is unstable toward spontaneous electron detachment (ADE = −0.41 eV). A similar isomer was found for Au$_3$BO$^-$ (C_s (^{2}A$'$) structure XIV, Figure 4c), but it is 39.3 kcal/mol higher than structure XI. The C_s (^{2}A$'$) structure XVII of H$_3$BO$^-$, which is 15.9 kcal/mol higher than the global minimum structure, can be considered as corresponding to both structures XI and XII of Au$_3$BO$^-$. While the C_s (^{2}A$'$) structure XV is another isomer of Au$_3$BO$^-$ with a relative energy of 40.4 kcal/mol, the similar structure XVIII C_s (^{2}A$'$) for H$_3$BO$^-$ is a first-order saddle point. The imaginary mode leads to the global minimum structure XVI. Two more similar structures are present among the isomers of Au$_3$BO$^-$ and H$_3$BO$^-$: C_s (^{2}A$''$) structure XIII (E_{relative} = 32.6 kcal/mol) and C_s (^{2}A$'$) structure XIX (E_{relative} = 21.5 kcal/mol), respectively (Figure 4c).

5. Interpretation of the Experimental Photoelectron Spectra

5.1. AuBO$^-$. The $C_{\infty v}$ ($^2\Sigma^+$) doublet ground state of AuBO$^-$ cluster has a valence electron configuration of $2\pi^4 1\delta^4 4\sigma^2 5\sigma^1$ and can give rise to either singlet or triplet final states upon electron detachment. The first calculated VDE corresponds to the removal of the unpaired electron from the 5σ orbital, resulting in the $^1\Sigma^+$ final state. The calculated VDE of 1.48 eV is in excellent agreement with the experimental value of 1.51 eV (Table 1). The calculated vibrational frequency for the Au−B stretching in neutral AuBO [$\omega_1(\sigma) = 430$ cm^{-1}] also agrees well with the resolved vibrational frequency for the ground state transition (430 ± 30 cm^{-1}). The second detachment channel involves the 4σ orbital (the HOMO of the neutral species) and leads to the $^3\Sigma^+$ final state. The computed VDE value of 4.56 eV agrees well with that of feature A at 4.78 eV (Table 1). There is another detachment channel for the 4σ orbital, which results in a singlet final state. The computed VDE (5.33 eV) for this detachment channel is in excellent agreement with the observed peak C (VDE = 5.26 eV). The relative intensity ratio of bands A and C and their similar shape are consistent with

a)

I, $C_{\infty v}$ ($^2\Sigma^+$)   II, $C_{\infty v}$ ($^2\Sigma^+$)   III, C_s ($^2A'$)

b)

IV   V   VI   VII   VIII   IX   X
$C_{\infty v}$ ($^1\Sigma^+$) C_{2v} ($^1A_1$) C_{2v} ($^1A_1$) $C_{\infty v}$ ($^1\Sigma^+$) $C_{\infty v}$ ($^1\Sigma^+$) C_s ($^1A'$) C_s ($^1A'$)

c)

XI   XII   XIII   XIV   XV
C_{2v} ($^2B_2$) C_s ($^2A'$) C_s ($^2A''$) C_s ($^2A'$) C_s ($^2A'$)

XVI   XVII   XVIII   XIX
C_s ($^2A'$) C_s ($^2A'$) C_s ($^2A'$) C_s ($^2A'$)
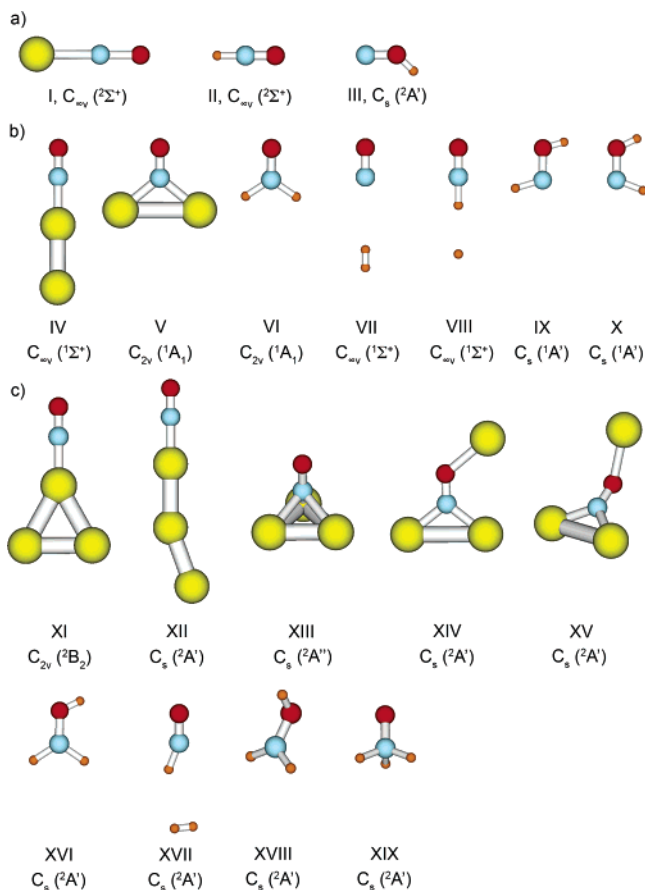
Figure 4. Structures of the most stable isomers of auro-borane oxides Au_nBO^- ($n = 1-3$) and boron hydride oxides H_nBO^- ($n = 1-3$): (a) $AuBO^-$ and HBO^-, (b) Au_2BO^- and H_2BO^-, and (c) Au_3BO^- and H_3BO^-.

the assignments that they are due to the triplet/singlet pair from detachment from the same orbital.

Detachments from deeper orbitals, which correspond to features B, D, and the congested signals at higher binding energies (Figure 1c), involve Au 5d-based orbitals and are complicated by the strong spin−orbit coupling (SOC) effect. The calculated VDEs for detachments from the 5σ and 4σ orbitals are in good agreement with the experiments because these two orbitals are mainly from the Au 6s orbital, which is not subject to the SOC effect. However, without including the SOC effect, the calculated electron detachment energies corresponding to removing electrons from the Au 5d-based 1δ and 2π orbitals are inconsistent with the experiment. Calculations of VDEs including the SOC effect are beyond the scope of the current work.

5.2. Au_2BO^-. The ground state of Au_2BO^- is a singlet with $C_{\infty v}$ ($^1\Sigma^+$) symmetry and possesses a closed shell configuration, $2\delta^4 3\pi^4 5\sigma^2 6\sigma^2$, which leads only to doublet final states upon electron detachment. The first detachment channel involves the 6σ orbital and the computed VDE of 4.08 eV is in good agreement with the ground state transition observed experimentally at 4.33 eV (Table 1). The observed band A (VDE: 5.31 eV) should correspond to detachment from the 5σ orbital and again computed VDE (5.19 eV) agrees well with the experimental VDE. The observed bands B and C should correspond to detachments from the 3π and 2δ orbitals, respectively. Even without including the SOC effect, the computed VDEs agree fortuitously well with the observed VDEs (Table 1). The SOC effect is expected to be relatively small for the $^2\Pi$ state because of the BO contribution to the 3π orbital. In fact, band B appeared

to contain two components with a shoulder on the higher binding energy side, which might be due to the spin−orbit splitting of the $^2\Pi$ state. However, the SOC effect of the $^2\Delta$ state is expected to be very large because the 2δ orbital is predominantly of Au 5d character. Thus, band C, which was fairly sharp, might correspond to one spin−orbit component of the $^2\Delta$ state with the other component at a higher binding energy beyond the 193 nm photon energy.

5.3. Au_3BO^-. The lowest energy structure of Au_3BO^- is C_{2v} ($^2B_2$) with an electron configuration of $3a_2^2 5b_2^2 9a_1^2 6b_2^1$, which can lead to both singlet and triplet final states upon electron detachment (Table 1). The ground state transition (X) should correspond to detachment from the $6b_2$ orbital and the calculated VDE (3.07 eV) is in excellent agreement with the experimental value of 3.13 eV (Table 1). The $6b_2$ orbital is an antibonding orbital between two Au atoms and the X band should contain an unresolved low-frequency Au−Au vibrational progression, which explains the difference between the ADE (3.08 eV) and VDE (3.13 eV) of the ground state transition (Figure 3 and Table 1). Band A should correspond to electron detachment from the $9a_1$ orbital leading to the triplet final state $^3B_2$. The corresponding $^1B_2$ singlet final state with a computed VDE of 4.90 eV (Table 1) should be then assigned to the B band at a VDE of 5.11 eV, which was only partially resolved from the more intense A band (Figure 3c). The next detachment channel is from the $5b_2$ orbital, resulting in the triplet $^3A_1$ (VDE: 5.34 eV) and singlet $^1A_1$ (VDE: 5.75 eV) final states. The computed VDEs are in good agreement with the observed VDEs of bands C and E, respectively (Table 1). The detachment from the $4b_2$-MO resulting in the $^3A_1$ final state could also contribute to feature E. The next higher binding energy photodetachment channel is from the $3a_2$ orbital, which gives rise to the triplet $^3B_1$ (VDE: 5.64 eV), which is in good agreement with the measured VDE for band D. Band F is more intense than band D, suggesting that it might contain contributions from many detachment channels. However, our assignment of the features D−F should be considered as tentative, because there are several close-lying VDEs in the range of these features.

The C_s ($^2A'$) isomer (structure XII, Figure 4c) of Au_3BO^- is very close in energy to the C_{2v} ($^2B_2$) ground state and might be present in experiment. Indeed, the calculated VDE from the $15a'$ SOMO of the C_s ($^2A'$) isomer is in reasonable agreement with the broad feature X′ observed at 266 nm (Figure 3b and Table 1). The contributions of the C_s ($^2A'$) isomer to the 193 nm spectrum (Figure 3c) appeared to be greatly diminished and should not interfere with the above assignments of the main isomer.

6. Chemical Bonding in Au_nBO^- and H_nBO^- ($n = 1-3$)

The overall agreement between the theory and experiment (Table 1) is gratifying for all three Au_nBO^- species, lending credence to the obtained global minimum structures. In this section, we discuss the details of the chemical bonding in Au_nBO^- and compare with that in the corresponding H_nBO^- and Au_nCO species for $n = 1-3$.

6.1. $AuBO^-$ and HBO^-. To simplify the analysis of the chemical bonding in the open-shell $AuBO^-$, we first consider the neutral AuBO species. Our NBO analysis of AuBO at the geometry of $AuBO^-$ is summarized in the Table S1 of the Supporting Information. The 5σ SOMO of $AuBO^-$ (Figure 5) becomes the LUMO of AuBO, whereas the 4σ orbital becomes the HOMO of the AuBO species. NBO analysis shows a relatively simple bonding picture in AuBO, because it involves only two-center two-electron (2c-2e) bonds and lone pairs.

Chemical Bonding of Au in Au$_n$BO$^-$ Clusters

J. Phys. Chem. A, Vol. 111, No. 9, 2007 **1653**

TABLE 2: Calculated Molecular Properties of the Lowest Energy Structures of Auro-Borane Oxides Au$_n$BO$^-$ (n = 1−3)

AuBO$^-$ $C_{\infty v}$ ($^2\Sigma^+$) B3LYP/SDD+AVTZ		Au$_2$BO$^-$ $C_{\infty v}$ ($^1\Sigma^+$) B3LYP/SDD+AVTZ	
$-E_{tot}$, au	236.150966	$-E_{tot}$, au	372.169882
R(B−O), Å	1.225	R(B−O), Å	1.222
R(Au−B), Å	2.061	R(Au$_1$−B), Å	2.013
		R(Au$_2$−Au$_1$), Å	2.659
		$\omega_1(\sigma)$, cm^{-1}	131 (3.2)[a]
$\omega_1(\sigma)$, cm^{-1}	328 (42.3)[a]	$\omega_2(\sigma)$, cm^{-1}	386 (16.4)[a]
$\omega_2(\sigma)$, cm^{-1}	1829 (270.3)[a]	$\omega_3(\sigma)$, cm^{-1}	1859 (354.0)[a]
$\omega_3(\pi)$, cm^{-1}	188 (43.0)[a]	$\omega_4(\pi)$, cm^{-1}	53 (4.6)[a]
		$\omega_5(\pi)$, cm^{-1}	356 (8.3)[a]

Au$_3$BO$^-$ C_{2v} (^{2}B$_2$) B3LYP/SDD+AVTZ		Au$_3$BO$^-$ C_s (^{2}A$'$) B3LYP/SDD+AVTZ	
$-E_{tot}$, au	508.111203	$-E_{tot}$, au	508.109561
R(B−O), Å	1.220	R(B−O), Å	1.219
R(Au$_1$−B), Å	2.004	R(Au$_1$−B), Å	2.010
R(Au$_{2,3}$−Au$_1$), Å	2.809	R(Au$_2$−Au$_1$), Å	2.715
$\angle$(Au$_2$Au$_1$Au$_3$), deg	57.8	R(Au$_3$−Au$_2$), Å	2.671
		$\angle$(Au$_3$Au$_2$Au$_1$), deg	160.0
$\omega_1(a_1)$, cm^{-1}	88 (0.4)	$\omega_1(a')$, cm^{-1}	13 (0.8)
$\omega_2(a_1)$, cm^{-1}	127 (0.5)	$\omega_2(a')$, cm^{-1}	89 (0.7)
$\omega_3(a_1)$, cm^{-1}	395 (6.0)	$\omega_3(a')$, cm^{-1}	141 (0.1)
$\omega_4(a_1)$, cm^{-1}	1869 (437.8)	$\omega_4(a')$, cm^{-1}	386 (21.8)
$\omega_5(b_1)$, cm^{-1}	50 (4.4)	$\omega_5(a')$, cm^{-1}	1873 (419.5)
$\omega_6(b_1)$, cm^{-1}	350 (7.2)	$\omega_6(a'')$, cm^{-1}	39 (4.4)
$\omega_7(b_2)$, cm^{-1}	30 (7.3)	$\omega_7(a'')$, cm^{-1}	41 (4.4)
$\omega_8(b_2)$, cm^{-1}	61 (0.2)	$\omega_8(a'')$, cm^{-1}	335 (7.2)
$\omega_9(b_2)$, cm^{-1}	336 (1.1)	$\omega_9(a'')$, cm^{-1}	335 (8.4)

[a] Infrared intensities (km/mol) are given in parentheses.

LUMO 6σ⁺   SOMO 5σ⁺   HOMO-1 4σ⁺   HOMO-2 2π   HOMO-3 1δ   HOMO-4 1π

HOMO-5 3σ⁺   HOMO-6 2σ⁺   HOMO-7 1σ⁺
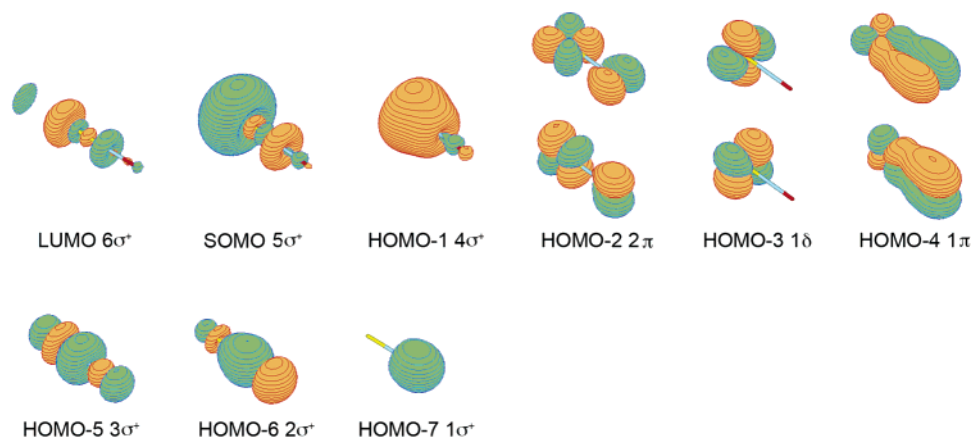
Figure 5. Molecular orbitals of AuBO$^-$ $C_{\infty v}$ ($^2\Sigma^+$).

There is a triple bond in the BO moiety and a single σ-bond between Au and BO. Five nearly pure d-character lone pairs are encountered on Au and one on oxygen. The charge distribution is as follows: −0.84 |e| on oxygen, 0.70 |e| on boron, and 0.14 |e| on gold, indicating a fairly strong covalent bond between Au and B with only a slight charge transfer from Au to BO.

In AuBO$^-$, the 5σ SOMO, which is pretty much the 6s AO of Au but with antibonding character in the Au−B fragment (Figure 5), is singly occupied. Our NBO analysis of the open-shell AuBO$^-$ (Table S2) shows that while the triple B−O bond, the lone pair at the oxygen, and the five lone pairs at the gold are preserved, the occupation number (OC) of the bonding orbital responsible for Au−B bond drops to only 1.00 |e| compared to 2.00 |e| in the neutral AuBO. The oxygen atom carries a negative charge of −0.96 |e|, and the Au and B have almost equal charges of opposite sign (−0.39 |e| and 0.35 |e|, respectively). The additional electron is almost equally distributed over the Au (0.53 |e|) and B (0.35 |e|) atoms with just 0.12 |e| acquired by O. The natural configuration of B is 2s$^{1.14}$-2p$^{1.42}$. So, in the ground state structure of AuBO$^-$, the Au atom

is still covalently bound to the B atom of the BO$^-$ fragment, though the chemical structure is halfway down to the elimination of the Au−B σ-bond and formation of a complex between Au and BO$^-$ similar to the bonding in AuCO.

The linear anionic HBO$^-$ (structure II, Figure 4a) is unstable and detachment of an electron lowers the energy of the system by approximately 13 kcal/mol. This is because the 5σ orbital in AuBO can easily accommodate an extra electron, whereas H in HBO does not possess an equivalent accepting property. Thus, the Au/H analogy still holds in neutral AuBO, but it reaches its limit in the anion due to the inability of hydrogen to accept any significant part of the extra electron.

6.2. Au$_2$BO$^-$ and H$_2$BO$^-$. We start our analysis of the chemical bonding in the Au$_2$BO$^-$ system by first considering the Au$_2$BO$^+$ cation, which has two electrons less than the anionic system. Reoptimization of the anionic structures of the $C_{\infty v}$ ($^1\Sigma^+$) isomer IV and C_{2v} (^{1}A$_1$) isomer V at the B3LYP/SDD+AVTZ level of theory shows that for the cation the $C_{\infty v}$ ($^1\Sigma^+$) structure becomes a second-order saddle-point and the C_{2v} (^{1}A$_1$) structure remains a local minimum. The same C_{2v} (^{1}A$_1$) local minimum cationic structure is achieved if the

LUMO 7a₁   HOMO 5b₂   HOMO-1 6a₁   HOMO-2 4b₂   HOMO-3 3b₁   HOMO-4 2a₂

HOMO-5 3b₂   HOMO-6 2b₂   HOMO-7 5a₁   HOMO-8 2b₁   HOMO-9 1a₂   HOMO-10 4a₁

HOMO-11 1b₁   HOMO-12 1b₂   HOMO-13 3a₁   HOMO-14 2a₁   HOMO-15 1a₁
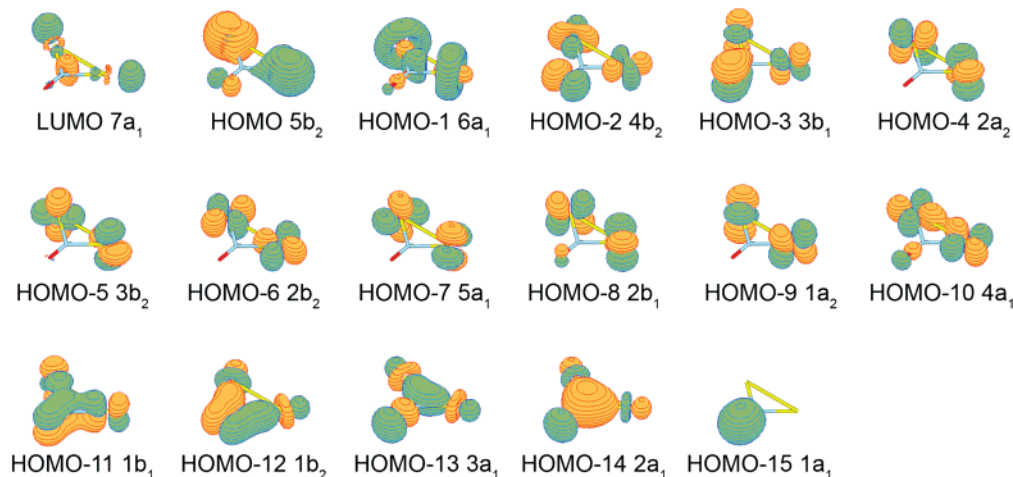
Figure 6. Molecular orbitals of Au_2BO^- C_{2v} ($^1A_1$).

imaginary mode of the $C_{\infty v}$ ($^1\Sigma^+$) cationic structure is followed. The geometry of the C_{2v} structure of the cation is more "compact" in the Au_2 fragment compared with the C_{2v} anion: the Au−Au distance is 2.664 Å in the cation vs 3.235 Å in the anion, the Au−B distance is 2.103 Å vs 2.098 Å, and the B−O distance is 1.207 Å vs 1.240 Å. These structural changes are understandable because the HOMO ($5b_2$) of the C_{2v} Au_2BO^- has strong Au−Au antibonding character (Figure 6). Molecular orbitals of the C_{2v} ($^1A_1$) Au_2BO^+ are similar to those of the C_{2v} ($^1A_1$) structure V of Au_2BO^- (Figure 6), except that the $5b_2$ orbital is no longer occupied in the cation. The 14 lowest occupied orbitals can be attributed to the triple B−O bond, the oxygen atom lone pair, and the ten lone pairs of the two gold atoms. Even though the d_{z^2} orbitals ($2a_1$ ad $3a_1$) have considerable contributions to the bonding of the Au_2B framework, the $6a_1$ orbital, which can be seen as a three-center two-electron (3c-2e) bond is mainly responsible for the bonding in the Au_2B fragment, rendering σ-aromaticity to the Au_2BO^+ cation. Indeed, our NBO analysis is consistent with this interpretation of the chemical bonding in the C_{2v} ($^1A_1$) structure of Au_2BO^+ (Table S3), revealing a 3c-2e bond with OC = 2.00 |e| between the two Au and the B atoms. The triple B−O bond, the lone pair of the oxygen, and the five lone pairs on each gold atom can be identified as well. NICS indexes calculated at the center of the Au_2B triangle support the assertion of aromaticity in Au_2BO^+: NICS(0) = −40.0 ppm, NICS(0.5) = −29.6 ppm, and NICS(1.0) = −13.8 ppm. The estimated interaction energy between the Au_2^+ and BO fragments in Au_2BO^+ is 85.1 kcal/mol at the B3LYP/SDD+AVTZ level of theory, indicating that they are indeed strongly bound by chemical bonding.

It is straightforward to understand the changes in the bonding pattern as a pair of electrons is added to Au_2BO^+ to form Au_2BO^-. There are two options to add the pair of electrons. The first option is to have the electron pair occupy the $5b_2$ orbital to yield the C_{2v} ($^1A_1$) isomer V of Au_2BO^-. Since the $5b_2$ is antibonding between the two gold atoms, the C_{2v} isomer of Au_2BO^- becomes antiaromatic. Consequently, two localized 2c-2e Au−B bonds are formed in Au_2BO^-, compared to one 3c-2e Au_2−B bond in Au_2BO^+. Our NBO analysis clearly shows that this is indeed the case (Table S4). Two Au−B bonds with OC = 1.74 |e| are formed now. The triple bond between oxygen and boron undergoes some minor changes. One of the π-bonds becomes more polarized toward oxygen and its occupation number drops from 1.95 |e| to 1.92 |e|. Its composition reveals some contribution of d- and f-functions (10% and 10%, respectively) on B in addition to p-functions (80%). The natural configuration of the boron atom is $2s^{0.80}2p^{1.66}$. Hence, the

polarized π-bond between boron and oxygen is actually a p-lone pair of oxygen. The antiaromaticity of the Au−B−Au fragment of the C_{2v} ($^1A_1$) structure V is confirmed by the obtained NICS values: NICS(0) = −15.0 ppm, NICS(0.5) = −11.3 ppm, and NICS(1.0) = −4.5 ppm.

Alternatively, the pair of electrons can occupy the $7a_1$ orbital (Figure 6), which is bonding between two gold atoms and antibonding between Au_2 and BO fragments. This occupation will cause the transformation of the 3c-2e Au_2−B bond into a lone pair on the boron atom and a 2c-2e Au−Au bond. Optimization of the C_{2v} structure with this electron configuration leads to a second-order saddle point, where the Au−Au, Au−B, and B−O distances become 2.547, 3.099, and 1.230 Å, respectively. NBO analysis of this system (Table S5) confirms that an Au−Au bond with OC = 1.97 |e| and a lone pair on the boron atom (OC = 1.92 |e|) are formed, instead of a 3c-2e Au_2−B bond. The presence of two imaginary normal modes can be attributed to the electrostatic instability of the system. Charge distribution shows that the Au_2 unit is almost electroneutral (total charge is −0.04 |e|; −0.02 |e| on each gold atom), while the OB^- unit has a dipole with a strongly negative charge of −1.03 |e| on the oxygen atom and an almost neutral boron atom (0.07 |e|). Following the largest imaginary mode, we found that the C_{2v} geometry transforms into the $C_{\infty v}$ ($^1\Sigma^+$) global minimum structure IV of Au_2BO^-. Results of the NBO analysis (Table S6) show that the charge is redistributed: the terminal gold atom has a negative charge of −0.63 |e|, the other gold atom is almost neutral with 0.06 |e|, the boron atom becomes significantly positive (0.52 |e|), and the oxygen basically preserves its negative charge (−0.94 |e|). In the neutral $C_{\infty v}$ species the charge on the terminal gold atom is 0.12 |e|, the other gold is almost neutral with 0.01 |e|, the charge on boron is 0.70 |e|, and that on oxygen is −0.84 |e|. Comparison of the charge distribution in the anionic vs neutral species clearly shows that the extra electron is almost completely acquired by the terminal gold atom (0.86 |e|). The natural configuration of the boron atom is $2s^{1.00}2p^{1.44}$ and the bonding pattern reflects these changes. The lone pair of the boron atom obviously transforms into the Au−B bond (OC = 2.00 |e|) and the Au−Au bond transforms into the sixth lone pair of the terminal gold atom (OC = 1.64 |e|). The low occupation number of this lone pair suggests that it possibly contributes to the bonding between the terminal Au^- and the AuBO unit. The estimated energy of this bond is 57.5 kcal/mol. The molecular orbitals of this isomer are presented at Figure 7. Indeed, the 6σ orbital is mainly responsible for the formation of the lone pair on the terminal Au, but it also has some bonding character in the Au−B region.

Chemical Bonding of Au in Au$_n$BO$^-$ Clusters

J. Phys. Chem. A, Vol. 111, No. 9, 2007 **1655**

| LUMO 7σ⁺ | HOMO 6σ⁺ | HOMO-1 5σ⁺ | HOMO-2 3π | HOMO-3 2δ | HOMO-4 4σ⁺ |

| HOMO-5 2π | HOMO-6 1δ | HOMO-7 1π | HOMO-8 3σ⁺ | HOMO-9 2σ⁺ | HOMO-10 1σ⁺ |
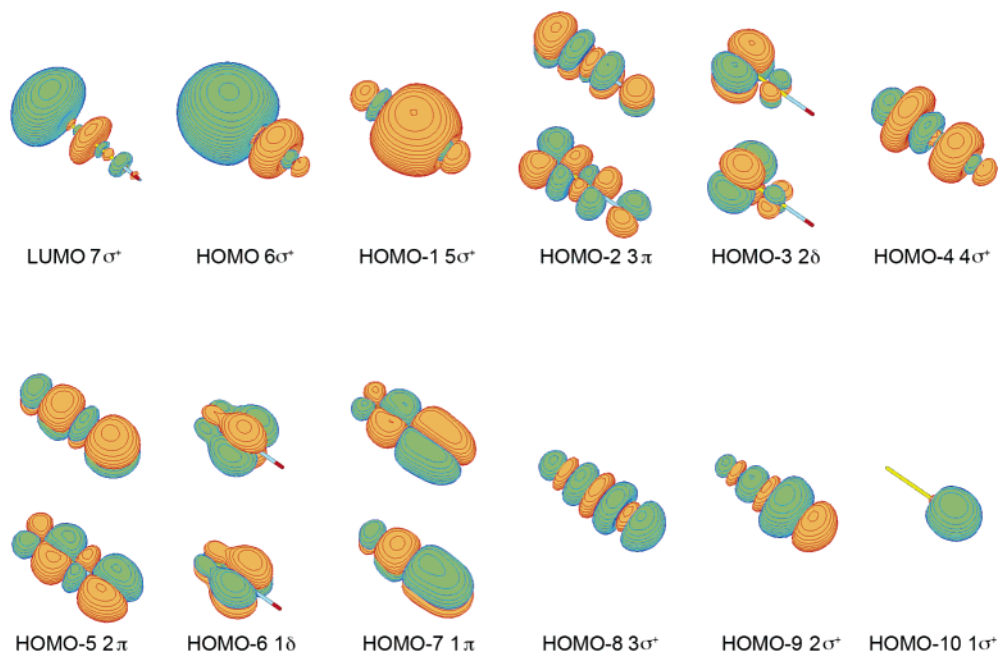
Figure 7. Molecular orbitals of Au$_2$BO$^-$ $C_{\infty v}$ ($^1\Sigma^+$).

| LUMO 10a₁ | SOMO 6b₂ | HOMO-1 9a₁ | HOMO-2 8a₁ | HOMO-3 5b₂ | HOMO-4 4b₂ |

| HOMO-5 3a₂ | HOMO-6 3b₂ | HOMO-7 2a₂ | HOMO-8 4b₁ | HOMO-9 7a₁ | HOMO-10 3b₁ |

| HOMO-11 6a₁ | HOMO-12 2b₂ | HOMO-13 1a₂ | HOMO-14 5a₁ | HOMO-15 2b₁ | HOMO-16 4a₁ |

| HOMO-17 1b₁ | HOMO-18 1b₂ | HOMO-19 3a₁ | HOMO-20 2a₁ | HOMO-21 1a₁ |
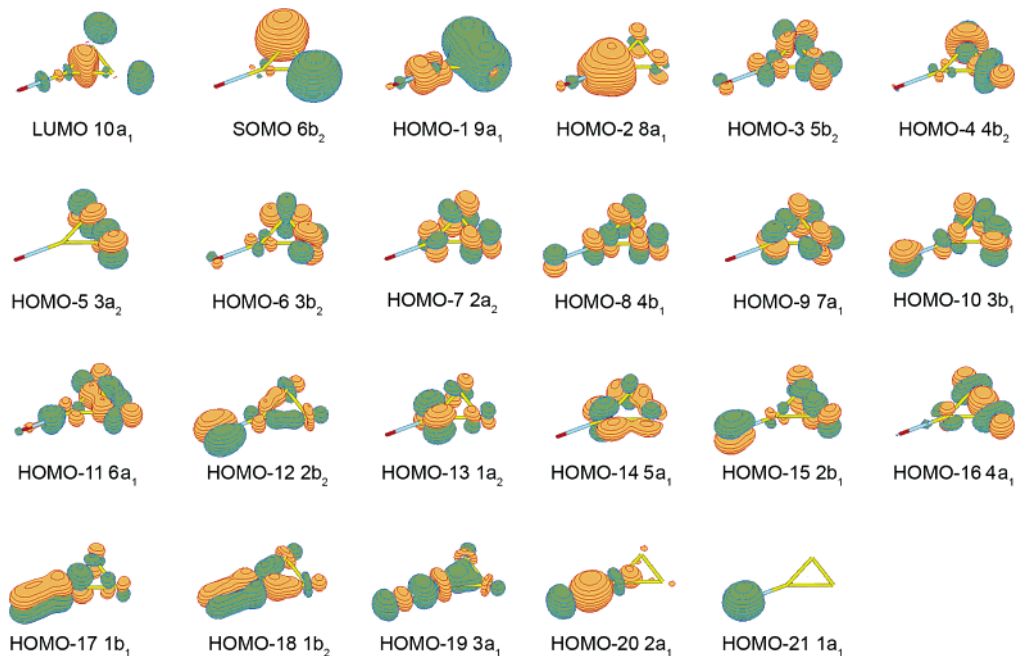
Figure 8. Molecular orbitals of Au$_3$BO$^-$ C_{2v} ($^2B_2$).

Second-order perturbation theory analysis available within NBO shows that there is significant donor–acceptor interaction between this lone pair and the low-occupation Au–B bond (OC = 0.34 |e|). So, the ground state $C_{\infty v}$ ($^1\Sigma^+$) isomer IV of Au$_2$BO$^-$ can be reasonably described as a stable neutral AuBO cluster bound with an Au$^-$ anion by a donor–acceptor interaction.

The C_{2v} ($^1A_1$) ground state structure of H$_2$BO$^-$ (structure VI, Figure 4b) is a classical molecule and has a very simple bonding pattern, which is confirmed by our NBO analysis. There is a double bond between oxygen and boron, two B–H bonds, a lone pair with contribution from s- and p-functions (44% and 56%, respectively), as well as an additional pure p-lone pair at the oxygen atom. The natural configuration of the boron atom is 2s$^{0.73}$2p$^{1.01}$3p$^{0.76}$. Interestingly, the comparison of the charge distribution in the anionic and neutral C_{2v} species shows that the extra electron is mainly acquired by oxygen (−0.99 |e| vs

−0.44 |e|) and the two hydrogen atoms (−0.24 |e| vs 0.00 |e|), while boron preserves its charge (0.47 |e| vs 0.44 |e|). So the stabilization of the extra charge occurs due to its delocalization, in contrast to the $C_{\infty v}$ isomer IV of Au$_2$BO$^-$, where the extra electron density is stabilized by the terminal gold atom.

6.3. Au$_3$BO$^-$ and H$_3$BO$^-$. The Au$_3$BO$^-$ cluster is also an open shell system so again we first consider the neutral C_{2v} Au$_3$BO with an electron removed from the SOMO of the C_{2v} ($^2B_2$) ground state (Figure 8). As shown in Figure 8, the 20 lowest molecular orbitals consist of a triple B–O bond, a single Au–B bond in the AuBO fragment, a lone pair at the oxygen atom, and five 5d lone pairs at each gold atom. The 9a₁ orbital accounts mainly for Au–Au bonding between the outer gold atoms. Thus Au$_3$BO can be described by a single Lewis structure, which is supported by our NBO analysis (Table S7). The expected bond between the outer gold atoms has OC equal

LUMO 16a'	SOMO 15a'	HOMO-1 14a'	HOMO-2 13a'	HOMO-3 12a'	HOMO-4 7a"
HOMO-5 11a'	HOMO-6 6a"	HOMO-7 10a'	HOMO-8 5a"	HOMO-9 9a'	HOMO-10 4a"
HOMO-11 8a'	HOMO-12 7a'	HOMO-13 3a"	HOMO-14 6a'	HOMO-15 2a"	HOMO-16 5a'
HOMO-17 1a"	HOMO-18 4a'	HOMO-19 3a'	HOMO-20 2a'	HOMO-21 1a'	
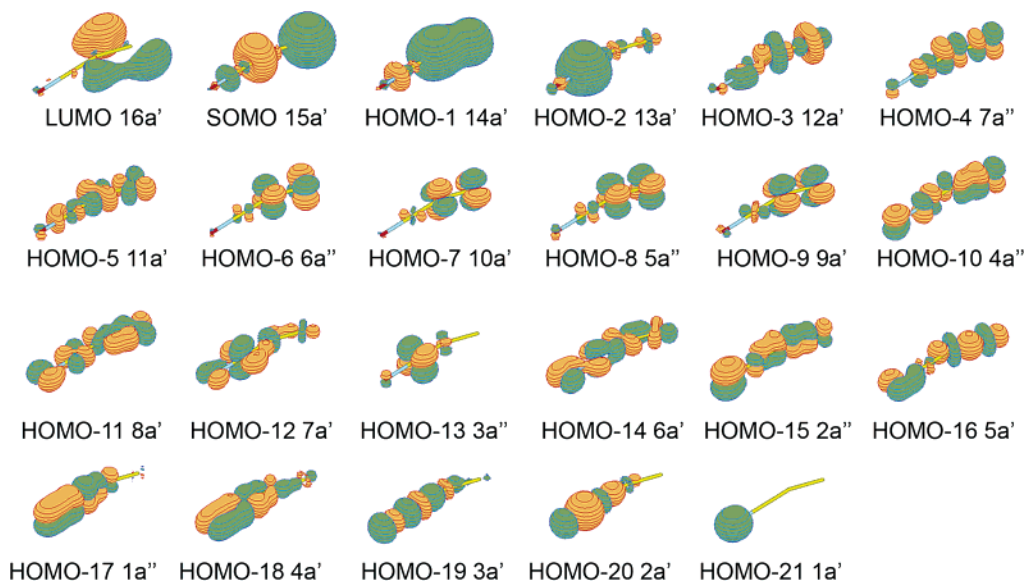
Figure 9. Molecular orbitals of Au_3BO^- C_s ($^2A'$).

to 1.76 |e| and the other bonding pairs all have OCs of 2 |e|. The natural configuration of the boron atom is $2s^{0.90}2p^{1.48}$. Therefore, the C_{2v} structure of Au_3BO can be represented as a complex of a Au_2 and a $AuBO$ unit. The Au_2 moiety carries a positive charge of 0.26 |e| equally distributed between the two atoms, and the $AuBO$ unit is a dipole with a total charge of −0.26 |e| [O: −0.85 |e|; B: +0.58 |e|; Au: +0.01 |e|]. Thus, Au_3BO can be viewed as a $Au_2[AuBO]$ complex. The estimated interaction energy between Au_2 and $AuBO$ is 23.0 kcal/mol.

In the anion Au_3BO^-, the extra electron occupies the $6b_2$ orbital (Figure 8), which is antibonding in the Au_2 moiety. Thus in Au_3BO^-, the bonding in the Au_2 unit will be weakened, but not eliminated completely, which is consistent with our NBO analysis of the C_{2v} ($^2B_2$) isomer of Au_3BO^- (Table S8). The additional electron (0.98 |e|) is equally distributed over the two Au atoms in the Au_2 unit. No changes occur in the bonding pattern of the $AuBO$ unit, but in the Au_2 unit the OC of the Au−Au bond is decreased to 0.88 |e|. The total charge on the Au_2 is −0.72 |e|, whereas that on the $AuBO$ unit is −0.29 |e|. Thus, the C_{2v} ($^2B_2$) isomer XI of Au_3BO^- can be considered as a complex of Au_2^- and $AuBO$, i.e., $Au_2^-[AuBO]$. The estimated interaction energy is 47.6 kcal/mol, which is twice as strong as the Au_2 and $AuBO$ interaction in Au_3BO. A second-order perturbation theory analysis shows significant interaction of the Au−Au bond (OC = 0.88 |e|) with the low-occupation Au−B bond in the $AuBO$ fragment (OC = 0.26 |e|).

Molecular orbitals of the low-lying C_s ($^2A'$) isomer XII of Au_3BO^- are presented in Figure 9. Interestingly, our analyses show that identical sets of orbitals are occupied for both isomers XI and XII, i.e., it is not a switch of orbitals from occupied and unoccupied spaces that causes distortion of the geometry from C_{2v} to C_s symmetry. The bonding pattern revealed by the NBO analysis (Table S9) supports this idea. Except for the charge redistribution, the C_s structure XII does not differ too much from the C_{2v} structure XI. We found that only low-occupancy lone pairs at the gold atoms of the Au_2^- unit contribute to the donor–acceptor interaction with $AuBO$ in the C_s isomer. The interaction energy is 47 kcal/mol, which is identical with that in the C_{2v} Au_3BO^-.

The open-shell C_s ($^2A'$) isomer XVI of H_3BO^- is electronically unstable. This explains the fact that the NBO analysis distributes one electron among several nonbonding orbitals, so that the bonding pattern in terms of lone pairs and 2c-2e bonds

is identical with one of the neutral C_s species: there is a double bond between O and B, two single H−B bonds, one single H−O bond, and a lone pair at the oxygen atom. The obtained picture of Lewis bonding is related to bonding in the C_{2v} ($^1A_1$) ground state structure VI of H_2BO^- described in the previous section, where one lone pair of the oxygen formed a bond with a proton. If compared with the neutral species, in the anion oxygen acquired 0.06 |e|, boron acquired 0.13 |e|, hydrogen atoms bound to boron acquired a total of 0.21 |e|, and the hydrogen atom bound to oxygen got 0.59 |e|. Once again, this demonstrates that hydrogen atoms in H_3BO^- cannot electrostatically stabilize an additional electron as Au atoms do in Au_3BO^-.

6.4. Au_nBO^- vs Au_nCO. Since BO^- is isoelectronic with CO, it is also interesting to compare the bonding between Au_nBO^- and Au_nCO. We computed the dissociation energies of Au_nBO^- to Au_n + BO^-, as follows:

$$AuBO^- \ (^2\Sigma^+) \rightarrow Au + BO^- \qquad \Delta E = 57.0 \text{ kcal/mol}$$

$$Au_2BO^- \ (^1\Sigma^+) \rightarrow Au_2 + BO^- \qquad \Delta E = 89.1 \text{ kcal/mol}$$

$$Au_3BO^- \ (^2B_2) \rightarrow Au_3 + BO^- \qquad \Delta E = 95.2 \text{ kcal/mol}$$

These interaction energies are significantly higher than the Au_nCO dissociation energies, which range from 18.4 kcal/mol for $n = 1$, to 35.2 kcal/mol for $n = 2$, to 37.3 kcal/mol for $n = 3$.[47] The structures of the Au_nBO^- clusters are similar to that of Au_nCO. The stronger interactions in Au_nBO^- are due to the charge on BO^-. From our chemical bonding analyses discussed above, we note that the Au_nBO^- clusters can all be viewed as $Au_n^-[BO]$, i.e., there is a significant charge transfer from BO^- to the Au_n clusters. This charge transfer is caused by the high electron affinities of the Au clusters. Charge transfer has also been observed to take place from CO to Au_n clusters in Au_nCO complexes and has been suggested to play a central role for understanding the catalytic mechanisms of low-temperature oxidation of CO on Au clusters and nanoparticles. Thus the Au_nBO^- clusters are not only interesting chemical species in their own right, but they are also interesting systems to provide insight into the CO interactions with Au clusters.

7. Conclusion

Anions of auro-boron oxides with composition Au_nBO^- ($n = 1$−3) have been observed in laser vaporization experiments

Chemical Bonding of Au in Au$_n$BO$^-$ Clusters

J. Phys. Chem. A, Vol. 111, No. 9, 2007 **1657**

intended to produce Au/B alloy clusters. The electronic structures and chemical bonding in these species have been investigated by photoelectron spectroscopy and theoretical calculations. Well-resolved photoelectron spectra were obtained at various photon energies and the electron affinities and low-lying electronic excited states of the neutral Au$_n$BO clusters were reported. Ground state structures of Au$_n$BO$^-$ were identified and confirmed by comparison with the experimental data. The structures and bonding of Au$_n$BO$^-$ were compared with the borane oxides H$_n$BO$^-$ ($n = 1-3$) to test the limit of the Au/H analogy. It was established that both AuBO$^-$ and Au$_2$BO$^-$ possess linear structures and Au$_3$BO$^-$ possesses a C_{2v} global minimum structure with a low-lying quasilinear C_s isomer. Molecular orbitals and NBO analyses showed that a single Au atom interacting with a bare BO unit indeed mimics hydrogen yielding a linear structure similar to that of HBO, though in anions HBO$^-$ is not stable because the H atom does not have an equivalent accepting property compared to Au in AuBO. The neutral AuBO fragment remains unchanged as the second and third Au atom is added to form Au$_2$BO$^-$ and Au$_3$BO$^-$. All the Au$_n$BO$^-$ species can also be viewed as Au$_n^-$[BO] complexes, i.e., there is a significant charge transfer from BO$^-$ to the Au clusters, analogous to that in Au$_n$CO complexes, although much stronger interaction exists in Au$_n$BO$^-$ due to the extra charge on BO$^-$.

Supporting Information Available: Tables of NBO analysis data for AuBO, AuBO$^-$, Au$_2$BO$^+$, Au$_2$BO$^-$, Au$_3$BO, and Au$_3$BO$^-$. This material is available free of charge via the Internet at http://pubs.acs.org.

References and Notes

(1) (a) Mitchell, C. M.; Stone, F. G. A. *J. Chem. Soc., Chem. Commun.* **1970**, 1263. (b) Reid, B. D.; Welch, A. J. *J. Organomet. Chem.* **1992**, *438*, 371. (c) Baukova, T. V.; Kuz'mina, L. G.; Dvortsova, N. V.; Porai-Koshits, M. A.; Kravtsov, D. N.; Perevalova, E. G. *Metalloorg. Khim.* **1989**, *2*, 1098. (d) Howard, J. A. K.; Jeffery, J. C.; Jelliss, P. A.; Sommerfeld, T.; Stone, F. G. A. *J. Chem. Soc., Chem. Commun.* **1991**, 1664. (e) Jeffery, J. C.; Jelliss, P. A.; Stone, F. G. A. *J. Chem. Soc., Dalton Trans.* **1993**, 1073. (f) Jeffery, J. C.; Jelliss, P. A.; Stone, F. G. A. *Inorg. Chem.* **1993**, *32*, 3943. (g) Jeffery, J. C.; Jelliss, P. A.; Stone, F. G. A. *Organometallics* **1994**, *13*, 2651. (h) Jeffery, J. C.; Jelliss, P. A.; Stone, F. G. A. *J. Chem. Soc., Dalton Trans.* **1994**, 25. (i) Harwell, D. E.; Mortimer, M. D.; Knobler, C. B.; Anet, F. A. L.; Hawthorne, M. F. *J. Am. Chem. Soc.* **1996**, *118*, 2679.

(2) (a) Hagen, S.; Pantenburg, I.; Weigend, F.; Wickleder, C.; Wesemann, L. *Angew. Chem., Int. Ed.* **2003**, *42*, 1501. (b) Marx, T.; Mosel, B.; Pantenburg, I.; Hagen, S.; Schulze, H.; Wesemann, L. *Chem. Eur. J.* **2003**, *9*, 4472. (c) Hagen, S.; Wesemann, L.; Pantenburg, I. *Chem. Commun.* **2005**, 1013.

(3) *Gold: Progress in Chemistry, Biochemistry and Technology*; Schmidbaur, H., Ed.; Wiley, Chichester, U.K., 1999; and references therein.

(4) Lauher, J. W.; Wald, K.; *J. Am. Chem. Soc.* **1981**, *103*, 7648.

(5) (a) Scherbaum, F.; Grohmann, A.; Muller, G.; Schmidbaur, H. *Angew. Chem., Int. Ed.* **1989**, *28*, 463. (b) Grohmann, A.; Riede, J.; Schmidbaur, H. *Nature* **1990**, *345*, 140. (c) Tamm, T.; Pyykkö, P. *Theor. Chem. Acc.* **2000**, *103*, 399. (d) Häberlen, O. D.; Schmidbaur, H.; Rösch, N. *J. Am. Chem. Soc.* **1994**, *116*, 8241. (e) Pyykkö, P.; Zhao, Y. *Chem. Phys. Lett.* **1991**, *177*, 103. (f) Blumenthal, A.; Beruda, H.; Schmidbaur, H. *J. Chem. Soc., Chem. Commun.* **1993**, 1005. (g) Shein, I. R.; Medvedeva, N. I.; Ivanovski, A. L. *Phys. Solid State* **2001**, *43*, 2213. (h) Yang, F.; Han, R. S.; Tong, N. H.; Guo, W. *Chin. Phys. Lett.* **2002**, *19*, 1336. (i) Parvin, F.; Islam, A. K. M. A.; Islam, F. N. *Solid State Commun.* **2004**, *130*, 567. (j) Kwon, S. K.; Min, B. I.; Youn, S. J.; Kim, K. S. *J. Korean Phys. Soc.* **2005**, *46*, L1295.

(6) Kiran, B.; Li, X.; Zhai, H. J.; Cui, L. F.; Wang, L. S. *Angew. Chem., Int. Ed.* **2004**, *43*, 2125.

(7) (a) Li, X.; Kiran, B.; Wang, L. S. *J. Phys. Chem. A* **2005**, *109*, 4366. (b) Kiran, B.; Li, X.; Zhai, H. J.; Wang, L. S. *J. Chem. Phys.* **2006**, *125*, 133204.

(8) Zhai, H. J.; Wang, L. S.; Zubarev, D. Yu.; Boldyrev, A. I. *J. Phys. Chem. A.* **2006**, *110*, 1689.

(9) Alexandrova, A. N.; Koyle, E.; Boldyrev, A. I. *J. Mol. Model.* **2006**, *12*, 569.

(10) Zubarev, D. Y.; Li, J.; Wang, L. S.; Boldyrev, A. I. *Inorg. Chem.* **2006**, *45*, 5269.

(11) (a) Thomas, C.; Wishart, B. J. *Theor. Chim. Acta* **1974**, *35*, 267. (b) Dill, J. D.; Schleyer, P. v. R.; Pople, J. A. *J. Am. Chem. Soc.* **1975**, *97*, 3402. (c) Summers, N. L.; Tyrrell, J. *J. Am. Chem. Soc.* **1977**, *99*, 3960. (d) Botschwina, P. *Chem. Phys.* **1978**, *28*, 231. (e) Tyrrell, J. *J. Phys. Chem.* **1979**, *83*, 2906. (f) Zyubina, T. S.; Charkin, O. P.; Gurvich, L. V. *Zh. Strukt. Khim.* **1979**, *20*, 3. (g) DeFrees, D. J.; Binkley, J. S.; McLean, A. D. *J. Chem. Phys.* **1984**, *80*, 3720. (h) Zyubina, T. S.; Zyubin, A. S.; Gorbik, A. A.; Charkin, O. P. *Zh. Neorg. Khim.* **1985**, *30*, 2739. (i) Peterson, K. A.; Woods, R. C. *J. Chem. Phys.* **1989**, *90*, 7239. (j) Page, M. *J. Phys. Chem.* **1989**, *93*, 3639. (k) Harrison, J. A.; Maclagan, R. G. A. R. *Chem. Phys. Lett.* **1989**, *155*, 419. (l) Talaty, E. R.; Huang, Y.; Zandler, M. E. *J. Am. Chem. Soc.* **1991**, *113*, 779. (m) Mains, G. J. *J. Phys. Chem.* **1991**, *95*, 5089. (n) Yamaguchi, Y.; Vacek, G.; DeLeeuw, B. J.; Richards, C. A.; Schaefer, H. F. *J. Chem. Phys.* **1994**, *101*, 3006. (o) Richards, C. A.; Vacek, G.; DeLeeuw, B. J.; Yamaguchi, Y.; Schaefer, H. F. *J. Chem. Phys.* **1995**, *102*, 1280. (p) Lory, E. R.; Porter, R. F. *J. Am. Chem. Soc.* **1971**, *93*, 6301. (q) Kawashima, Y.; Kawaguchi, K.; Hirota, E. *Chem. Phys. Lett.* **1986**, *131*, 205. (r) Kawashima, Y.; Endo, Y.; Kawaguchi, K.; Hirota, E. *Chem. Phys. Lett.* **1987**, *135*, 441. (s) Kawashima, Y.; Endo, Y.; Hirota, E. *J. Mol. Spectrosc.* **1989**, *133*, 116.

(12) (a) Haruta, M.; Yamada, N.; Kobayashi, T.; Iijima, S. *J. Catal.* **1989**, *115*, 301. (b) Haruta, M.; Tsubota, S.; Kobayashi, T.; Kageyama, H.; Genet, M. J.; Delmon, B. *J. Catal.* **1993**, *144*, 175.

(13) (a) Haruta, M. *Catal. Today* **1997**, *36*, 153. (b) Haruta, M. *Chem. Rec.* **2003**, *3*, 75. (c) Bond, G. C.; Thompson, D. T. *Catal. Rev. Sci. Eng.* **1999**, *41*, 319.

(14) (a) Valden, M.; Lai, X.; Goodman, D. W. *Science* **1998**, *281*, 1647. (b) Chen, M. S.; Goodman, D. W. *Science* **2004**, *306*, 252.

(15) Iizuka, Y.; Tode, T.; Takao, T.; Yatsu, K. I.; Takeuchi, T.; Tsubota, S.; Haruta, M. *J. Catal.* **1999**, *187*, 50.

(16) (a) Kim, T. S.; Stiehl, J. D.; Reeves, C. T.; Meyer, R. J.; Mullins, C. B. *J. Am. Chem. Soc.* **2003**, *125*, 2018. (b) Stiehl, J. D.; Kim. T. S.; McClure, S. M.; Mullins, C. B. *J. Am. Chem. Soc.* **2004**, *126*, 1606.

(17) (a) Guzman, J.; Gates, B. C. *Nano Lett.* **2001**, *1*, 689. (b) Guzman, J.; Gates, B. C. *J. Am. Chem. Soc.* **2004**, *126*, 2672.

(18) Date, M.; Okumura, M.; Tsubota, S.; Haruta, M. *Angew. Chem., Int. Ed.* **2004**, *43*, 2129.

(19) Lemire, C.; Meyer, R.; Shaikhutdinov, S.; Freund, H. J. *Angew. Chem., Int. Ed.* **2004**, *43*, 118.

(20) Liu, Z. P.; Hu, P.; Alavi, A. *J. Am. Chem. Soc.* **2002**, *124*, 14770.

(21) Molina, L. M.; Hammer, B. *Phys. Rev. Lett.* **2003**, *90*, 206102.

(22) (a) Sanchez, A.; Abbet, S.; Heiz, U.; Schneider, W. D.; Hakkinen, H.; Barnett, R. N.; Landman, U. *J. Phys. Chem. A* **1999**, *103*, 9573. (b) Yoon, B.; Hakkinen, H.; Landman, U.; Wirz, A. S.; Antonietti, J. M.; Abbet, S.; Heiz, U. *Science* **2005**, *307*, 403.

(23) Lee, S.; Fan, C.; Wu, T.; Anderson, S. L. *J. Am. Chem. Soc.* **2004**, *126*, 5682.

(24) (a) Mavrikakis, M.; Stoltze, P.; Norskov, J. K. *Catal. Lett.* **2000**, *64*, 101. (b) Lopez, N.; Janssens, T. V. W.; Clausen, B. S.; Xu, Y.; Mavrikakis, M.; Bligaard, T.; Norskov, J. K. *J. Catal.* **2004**, *223*, 232.

(25) Nygren, M. A.; Siegbahn, P. E. M.; Jin, C.; Guo, T.; Smalley, R. E. *J. Chem. Phys.* **1991**, *95*, 6181.

(26) Lee, T. H.; Ervin, K. M. *J. Phys. Chem.* **1994**, *98*, 10023.

(27) Wallace, W. T.; Whetten, R. L. *J. Phys. Chem. B* **2000**, *104*, 10964.

(28) (a) Balteanu, I.; Balaj, O. P.; Fox, B. S.; Beyer, M. K.; Bastl, Z.; Bondybey, V. E. *Phys. Chem. Chem. Phys.* **2003**, *5*, 1213. (b) Fielicke, A.;

von Helden, G.; Meijer, G.; Pedersen, D. B.; Simard, B.; Rayner, D. M. *J. Am. Chem. Soc.* **2005**, *127*, 8416.

(29) (a) Liang, B.; Andrews, L. *J. Phys. Chem. A* **2000**, *104*, 9156. (b) Jiang, L.; Xu, Q. *J. Phys. Chem. A* **2005**, *109*, 1026.

(30) Zhai, H. J.; Wang, L. S. *J. Chem. Phys.* **2005**, *122*, 051101.

(31) Zhai, H. J.; Kiran, B.; Dai, B.; Li, J.; Wang, L. S. *J. Am. Chem. Soc.* **2005**, *127*, 12098.

(32) Wang, L. S.; Wu, H. Probing the electronic structure of transition metal clusters from molecular to bulk-like using photoelectron spectroscopy. In *Advances in Metal and Semiconductor Clusters. IV. Cluster Materials*; Duncan, M. A., Ed.; JAI Press: Greenwich, CT, 1998; pp 299−343.

(33) Wang, L. S.; Cheng, H. S.; Fan, J. *J. Chem. Phys.* **1995**, *102*, 9480.

(34) (a) Parr, R. G.; Yang, W. *Density-functional theory of atoms and molecules*; Oxford University Press: Oxford, UK, 1989. (b) Becke, A. D. *J. Chem. Phys.* **1993**, *98*, 5648. (c) Perdew, J. P.; Chevary, J. A.; Vosko, S. H.; Jackson, K. A.; Pederson, M. R.; Singh, D. J.; Fiolhais, C. *Phys. Rev. B* **1992**, *46*, 6671.

(35) Hay, P. J.; Wadt, *J. Chem. Phys.* **1985**, *82*, 299.

(36) (a) Dolg, M.; Wedig, U.; Stoll, H.; Preuss, H. *J. Chem. Phys.* **1987**, *86*, 866. (b) Martin, J. M. L.; Sundermann, A. *J. Chem. Phys.* **2001**, *114*, 3408.

(37) (a) Dunning, T. H., Jr. *J. Chem. Phys.* **1989**, *90*, 1007. (b) Woon, D. E.; Dunning, T. H., Jr. *J. Chem. Phys.* **1993**, *98*, 1358. (c) Kendall, R. A.; Dunning, T. H., Jr.; Harrison, R. J. *J. Chem. Phys.* **1992**, *96*, 6796. (d) Peterson, K. A.; Woon, D. E.; Dunning, T. H., Jr. *J. Chem. Phys.* **1994**, *100*, 7410. (e) Wilson, A.; van Mourik, T.; Dunning, T. H., Jr. *J. Mol. Struct.* (*THEOCHEM*) **1997**, *388*, 339. (f) Davidson, E. R. *Chem. Phys. Lett.* **1996**, *220*, 514.

(38) (a) Bauernshmitt, R.; Alrichs, R. *Chem. Phys. Lett.* **1996**, *256*, 454. (b) Casida, M. E.; Jamorski, C.; Casida, K. C.; Salahub, D. R. *J. Chem. Phys.* **1998**, *108*, 4439.

(39) (a) Li, J.; Li, X.; Zhai, H. J.; Wang, L. S. *Science* **2003**, *299*, 864. (b) Li, X.; Kiran, B.; Li, J.; Zhai, H. J.; Wang, L. S. *Angew. Chem., Int. Ed.* **2002**, *41*, 4786.

(40) Glendening, E. D.; Badenhoop, J. K.; Reed, A. E.; Carpenter, J. E.; Bohmann, J. A.; Morales, C. M.; Weinhold, F. *NBO 5.0*; Theoretical Chemistry Institute, University of Wisconsin: Madison, WI, 2001.

(41) Frisch, M. J.; et al. *Gaussian 03*, revision A.1; Gaussian, Inc.: Pittsburgh, PA, 2003.

(42) Aprá, E.; et al. *NWChem 4.7*, NWChem, A Computational Chemistry Package for Parallel Computers, Version 4.7; Pacific Northwest National Laboratory: Richland, WA, 2005.

(43) Schaftenaar, G. *MOLDEN 3.4*; CAOS/CAMM Center, The Netherlands, 1998.

(44) (a) Hakkinen, H.; Yoon, B.; Landman, U.; Li, X.; Zhai, H. J.; Wang, L. S. *J. Phys. Chem. A* **2003**, *107*, 6168. (b) Taylor, K. J.; Pettiette-Hall, C. L.; Cheshnovsky, O.; Smalley, R. E. *J. Chem. Phys.* **1992**, *100*, 7093.

(45) (a) Zhai, H. J.; Alexandrova, A. N.; Birch, K. A.; Boldyrev, A. I.; Wang, L. S. *Angew. Chem., Int. Ed.* **2003**, *42*, 6004. (b) Zhai, H. J.; Kiran, B.; Li, J.; Wang, L. S. *Nat. Mater.* **2003**, *2*, 827.

(46) Gutsev, G. L.; Boldyrev, A. I. *Adv. Chem. Phys.* **1985**, *61*, 169.

(47) Wu, X.; Senapati, L.; Nayak, S. K.; Selloni, A.; Hajaligol, M. *J. Chem. Phys.* **2002**, *117*, 4010.